CHINESE JOURNAL OF PHYSICS VOL. 25, NO. 3 AUTUMN 1987

Fundamentals of The Recording Head Fields*

Huei Li Huang (黃暉理), Chia Shen Wang (王嘉申)
and
Jyh Shinn Yang (楊志信)
Department of Physics, National Taiwan University, Taiwan

(Received April 25, 1987)

Various approximation schemes in head field calculations for conventional ring heads and thin film heads for longitudinal recording and pole keeper heads for vertical recording and, to a lesser extent, the readout waveform of the magnetoresistive heads are broadly discussed. Relative merits, demerits and the precision of each calculation method are also briefly discussed.

* An invited review presented at the 3rd Annual Symposium on Magnetism and Magnetic Materials held in Taipei, April 1987.

I. INTRODUCTION

There are two key areas of interest in the physics of magnetic recording. One is the recording (writing) process. The other is the reproducing (playback) process. The recording processes is a highly nonlinear process, which has been a subject of much discussion from investigators around the world recently. Yet none of the non-linearity of the problem, neither the functional dependence of the magnetization transition width nor the in-depth distribution of it, is well understood; let alone the complicated behaviour of the hysteresis minor loop patterns. The reproducing process is comparatively less complicated; in that researchers are capable of analyzing the reproduce waveform through the use of the reciprocity theorem, once the structure of the recorded pattern of the magnetization transition is known. An in-depth understanding of the recording head field function is usually a prerequisite, though not sufficient, to the study of the recording and/or reproducing process. In this paper we report various approximation schemes whereby the magnitude and characteristic behaviour of the head field function in relation to the conventional ring heads and vertical pole type heads will be broadly discussed and summarized, then follow

this by a new method of thin film head fields calculation. Finally, to a lesser extent the reproduce waveform of the magneoresistive heads will also be briefly discurred. Hysteretic behaviour of magnetic media will not be covered in this short article.

II. RING HEADS

The essence of a ring head is shown in Fig. 1. Typically it consists of a highly permeable magnetic core in a ring shape carrying N number of turns of current I and an air gap of length g. Following Ampere's law one obtains

$$\mathbf{H} \cdot \mathrm{dl} = \mathrm{NI} \tag{1}$$

or

$$H_0\, g + H_c\, l = \mathrm{NI} \tag{1}'$$

where H_0 is the field strength along the path within the gap, H_c is the field strength within the core, g is the gap length and 1 the path length within the core. From any elementary textbook on magnetic circuits, H_c is practically zero inside a highly permeable magnetic core. Thus

$$H_0 \cong \mathrm{NI}/g \tag{2}$$

which is equivalent to the magnetizing field from a wire of NI windings evaluated at a distance $g/2\pi$ from the wire center.

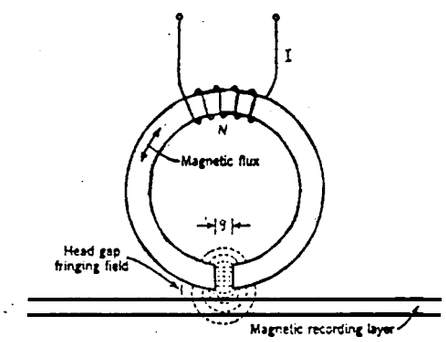

FIG. 1 Structure of a conventional ring head.

The flux paths, at the distance from the gap above the head surface where the medium passes, are roughly semi-circular in shape.[1a] Thus, if the integrating path is taken along this

semi-circular path, one obtains the alternative expression

$$H = \frac{NI}{\pi r} \tag{3}$$

or

$$H_x = \frac{NIy}{\pi(x^2 + y^2)}, \qquad H_y = -\frac{NIx}{\pi(x^2 + y^2)} \tag{3)'}$$

Note that the field from a wire of NI windings evaluated at a distance r from the wire center gives only half this value. The field components H_x and H_y are known as the longitudinal component and vertical component respectively.

A more rigorous treatment of the ring head field calls for *a more* sophisticated approach. Typically, a conformal mapping technique is used to calculate the field in the close vicinity of the head gap[2]. A simpler alternative approach is to solve the 2-dim Laplace equation with a 2-dim Green function[3] to obtain:

$$H_x = \frac{H_0}{\pi}\left\{\tan^{-1}\frac{g/2 + x}{y} + \tan^{-1}\frac{g/2 - x}{y}\right\} \tag{4a}$$

$$H_y = \frac{H_0}{2\pi}\ln\frac{(g/2 - x)^2 + y^2}{(g/2 + x)^2 + y^2} \tag{4b}$$

where H_0 is the deep gap field as given above. In obtaining (4a) and (4b) the following simplified approximations are generally made: First, the toroidal core is assumed to be infinitely permeable so that there is no potential drop within the toroid. Second, the potential is assumed to vary linearly across the gap. The first approximation invariably leads to constancy in magnetic potential, yielding a zero x-component of the field, $H_x = 0$, on the head surface but not along the gap face. Both approximations involve an error which is relatively negligible if the head-to-media spacing is on the order of the gap length g. The error however, becomes increasingly significant when the spacing is only a small fraction of the gap length, say 0.2g or less.

To obtain an exact head field distribution for an infinitely permeable head, fan Employed a Fourier series expansion and the, Fourier integral method[4]. Referring to Fig. 2,

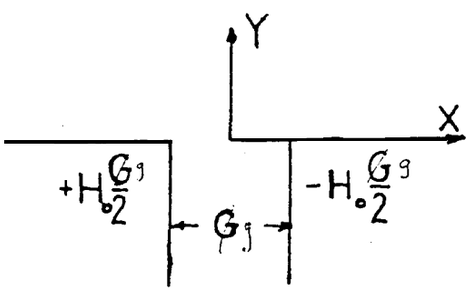

FIG. 2 Schematic diagram of a ring head: g: gap width, $H_0 g$: potential drop across the gap.

we expand a ring head with potential difference $-H_0\, g/2$ and $H_0\, g/2$ between a gap length g in a Fourier series [5,6] to obtain

$$H_{Rx} = H_0 + \sum_{n=1}^{\infty} A_n\, n\pi \cos(2n\pi x/g) e^{2n\pi y/g}, \quad 0 \leqslant x \leqslant g/2,\ y \leqslant 0 \quad , \tag{5a}$$

$$H_{Rx} = \frac{H_0}{\pi}\left[\tan^{-1}\left(\frac{x + g/2}{y}\right) - \tan^{-1}\left(\frac{x - g/2}{y}\right)\right] +$$

$$\sum_{n=1}^{\infty} 2n(-)^n\, A\, n \int_0^{\infty} \frac{k \sin kg/2 \cos kx}{k^2 - (2n\pi/g)^2} e^{-ky}\, dk,\ 0 \leqslant x, \quad 0 \leqslant y$$

$$= H_{Rx}^K + H_{Rx}^C \tag{5b}$$

Similarly,

$$H_{Ry} = \sum_{n=1}^{\infty} An\ n\pi\ \sin\frac{2n\pi x}{g}\ e^{2n\pi y/g}, \quad 0 \leqslant x \leqslant g/2,\ y \leqslant 0 \tag{6a}$$

$$H_{Ry} = \frac{H_0}{2\pi} \ln \frac{y^2 + (x - g/2)^2}{y^2 + (x + g/2)^2} +$$

$$\sum_{n=1}^{\infty} An\ 2n(-)^{n+1} \int_0^{\infty} \frac{k \sin kg/2\ \sin kx}{k^2 - (2n\pi/g)^2} e^{-ky}\, dk, \quad 0 \leqslant x, \quad 0 \leqslant y \tag{6b}$$

$$= H_{Ry}^K + H_{Ry}^C$$

where H_{Rx}^K is the Karlquist field, H_{Rx}^C characterizes the extent of correction from the Karlquist field, H_{Ry}^K and H_{Ry}^C are interpreted similarly, and Am satisfies the relation

$$\frac{Am}{2} = \frac{2}{\pi}(-)^{m+1}\left[\sum_{n=1}^{\infty} An(-)^n\, n\pi K_{nm} + H_0\, Lm\right] \tag{7}$$

in which K_{nm} and Lm have been defined elsewhere[4].

To get a feeling for the magnitude of the correction term H_{RX}^C relative to the Karlquist field one needs to evaluate the coefficients An. Also, the convergence of the head field distribution, that is the number of terms which need be retained in the Fourier series, depends sensitively on the closeness of the spacing. For $y/g \geqslant 0.2$, ten terms suffice; at lower spacings 40 or even 100 terms are required, in which a matrix of 40 X 40 or higher dimension has to be dealt with. Typical An-values for n = 10 are A_1 = -0.85715, A_2 = 0.028822, A_3 = -0.014987, A_4 = 0.009365, A_5 = -0.007481, A_6 = 0.004788, A, = -0.003701, A_8 = 0.002958, A_9 = -0.002425, A_{10} = 0.002029. These ten An-values do not change very much with a change in the number of terms retained. However, the head field undulates

visibly within the gap region if insufficient terms are retained. Figure 3 shows the ring head write field distribution for n = 24 based on Eqs. (5a) and (5b) (curve A) accompanied by the Karlquist field (curve B) and the relative correction term (curve C) at y/g = 0.1.

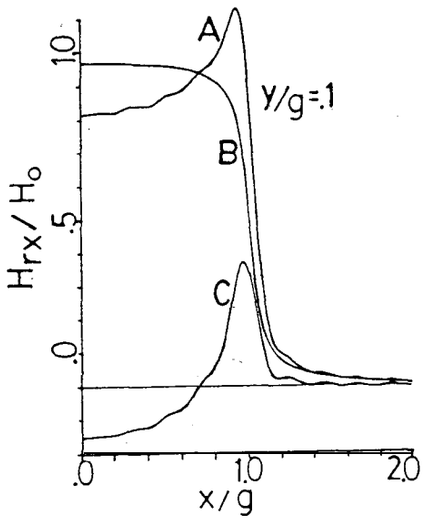

FIG. 3 Curve A: ring head write field distribution at y/g = 0.1 when 24 An ' s are retained. Curev B: Karlquist head field; Curve C: Difference between area A and B.

Despite the accuracy of the above numerical calculation it seems too cumbersome to suit practical needs. To overcome this short-coming Szczech and co-workers (SSP) derived a three-parameter formula[7] which is highly capable of reproducing the fine features shown in curve A of Fig. 3. Employing a contour integral in the half-space above the head surface known as the Poisson integral the head field components can be expressed as

$$H_{RX}(x, y) = \int_{-\infty}^{\infty} H_{RX}(t, 0)\, K_1(t\text{-}x, Y)\, dt \tag{8a}$$

$$H_{Ry}(x, y) = \int_{-\infty}^{\infty} H_{RX}(t, 0)\, K_2(t\text{-}x, Y)\, dt \tag{8b}$$

where

$$K_1(t-x, y) = \frac{1}{\pi} \frac{y}{(t-x)^2 + y^2},$$

$$K_2(t-x, y) = \frac{-1}{\pi} \frac{x-t}{(t-x)^2 + y^2} \tag{8c}$$

are the equivalent kernel functions and $H_{RX}(t, 0)$ is the x-component ring head field at the gap face given by the parametric equation

$$H_{RX}(t, 0) = \left[A + \frac{Bg^2}{[(cg)^2 - t^2]}\right] H_s \tag{9}$$

in which $H_s \equiv H_{RX}$ (0, 0), g is the gap length and A, B and C are the parameters. Szczech and co-workers used a finite difference method to obtain the numerical values of the surface gap field, allowing least square fitting of the parameters, A, B, C and H_s. Although different numerical methods may lead to slightly different values of the parameters, A, B, C and H_s they nonetheless yield essentially the same head field distributions[8,9]. Table I lists the numerical values of the parameters corresponding to n = 100, 200 in the Fourier series

TABLE I. Numerical values of the surface gap field parameters of ring heads

	N = 30	100	200	SPP[a]	FEM
A	0.855 1	0.8917	0.9196	0.835	0.9063
B	0.03659	0.03017	0.02729	0.0433	0.03055
C	0.5123	0.5080	0.5057	0.512	0.5098
H_s	—	0.8406	0.8380	0.83	0.8402

a = Ref. 7

expansions, the results obtained by Szezech and co-workers (SSP) and those obtained by the finite element method (FEM). Figure 4 shows the comparison of the x-component ring head field distribution based on the parameters obtained for n = 200, SPP, FEM and the field from direct finite element calculation, denoted as FEM (direct).

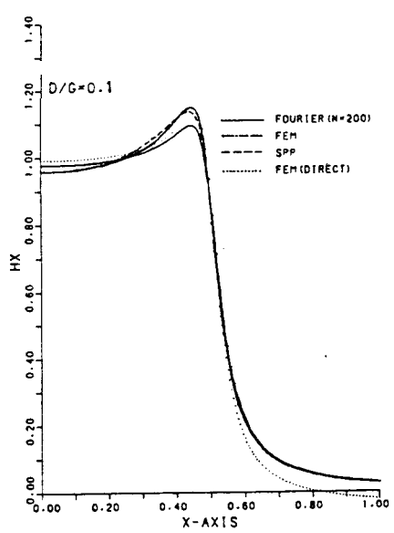

FIG. 4 Comparison of the x-component field at y/g = 0.05 based on the parameters N = 200, FEM, SPP and from direct FEM calculation.

III. POLE TYPE HEADS

To avoid ambiguity, it is necessary to begin this section by defining what is meant by a pole type head in the context of the vertical recording. By a pole type head we mean a single pole piece in coupling with a high permeability keeper layer which serves as an image plane for the, former. With this definition it is easy to see that the pole type head field can also be solved using the Fourier series and Fourier integral method", as in the case of the ring head. With some modification, the head field of pole thickness p (see Fig. 5) can be expressed as[5,6]

$$H_{px} = \sum_{n\,r\,l}^{\infty} B_n n\pi \sin\frac{n\pi y}{d} \sinh n\pi\left(\frac{x + p/2}{d}\right), -p/2 < x \leqslant 0,\ 0 \leqslant y \leqslant d, \tag{9a}$$

$$= \frac{H_0}{2\pi} \ln\frac{x^2 + (y-d)^2}{x^2 + (y+d)^2} + \sum_{n=l}^{\infty} Bn\pi\cos\left(\frac{n\pi p}{2d}\right)$$

$$X\ 2n(-)^{n+1} \int_0^{\infty} \frac{k\ \sinh kd \sinh kx}{k^2 - \left(\frac{n\pi}{d}\right)^2} e^{-ky}\,dk$$

$$= H_{px}^{k} + H_{px}^{c}, \qquad 0 \leqslant x,\quad 0 \leqslant y\ ; \tag{9b}$$

$$H_{py} = H_0 + \sum_{n=l}^{\infty} Bn\ n\pi\cos\left(\frac{n\pi y}{d}\right) \cosh n\pi\left(\frac{x + p/2}{d}\right), -p/2 < x \leqslant 0,\ 0 \leqslant y \leqslant d \tag{10a}$$

$$= \frac{H_0}{\pi}\left[\tan^{-1}\left(\frac{y+d}{x}\right) - \tan^{-1}\left(\frac{y-d}{x}\right)\right] +$$

$$\sum_{n=l}^{\infty} Bn\ \cosh n\pi\left(\frac{x + P/2}{d}\right) 2n(-)^n \int_{,}^{\infty} \frac{k \sinh kd \cos kx}{k^2 - \left(\frac{n\pi}{d}\right)^2} e^{-ky}\,dk,\ x \geqslant 0,\ y \geqslant 0$$

$$= H_{py}^{K} + H_{py}^{C} \tag{10b}$$

where H_{py}^{k} and H_{py}^{c} have the same meaning as noted earlier (now for a pole type head) and d is the head-to-media spacing. The coefficients B_n satisfy the relation

$$\frac{B_m}{2} \sinh\left(\frac{m\pi p}{2d}\right) =$$

$$\frac{2}{\pi}(-)^{m+1}\left[\sum_{n=1}^{\infty}(-)^n B_n \cosh\left(\frac{n\pi p}{2d}\right) K_{nm} n\pi + H_0 Lm\right], \tag{11}$$

Comparison of Eqs. (5) and (10) suggests that the x-component ring head write field and y-component pole type head write field appear to behave somewhat similarly". A closer-look at the coefficients shows that by introducing a new coefficient $A_n' = B_n \cosh\left(\frac{n\pi p}{2d}\right)$ we find

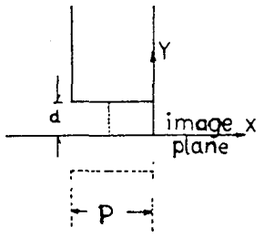

FIG. 5 Schematic diagram of a pole type head; P: thickness of the pole piece.

that Eq. (1 1) reduces exactly to Eq. (7) in the limit of p/d >> 1, and Eq. (5b) becomes formally identical to Eq. (10b). Note carefully, however, that the *two* equations refer to different write field spaces-they are never actually identical to each other. Figure 6 shows the variation of the y-component pole type head write field parallel to its image plane for

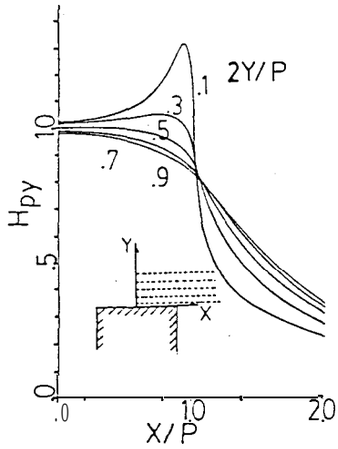

FIG. 6 Variation of the y-component pole type head write field parallel to its image plane for several spacings, 2y/p = 0.1, 0.3, 0.5, 0.7 and 0.9 at d = p/z.

several flying heights, 2y/p = 0.1, 0.3, 0.5, 0.7 and 0.9. Comparison of the ring head write field versus pole type head write field is shown in Fig. 7. Curve A is for H_{Rx} vs y/g, parallel to its image plane. Curve B is for H_{py} vs x/p (for p = g), along the direction of the media motion. Curve C is for H_{Rx} vs x/g, along the direction of the media motion. The two curves A and B are equivalent from either field symmetry or geometry considerations.[12] The slight difference between the two curves A and B results primarily from the fact that the pole piece of a ring head is semi-infinite in extent while for a pole type head the pole thickness is small but finite. In a real physical world where a ring head is made up of a finite pole tip along the y-direction, the two curves A and B may approximate even more closely to each other, except that the curve A perhaps will never be measured, nor will it be useful. The write field of a ring head with a finite pole piece L along the y-direction calls for a

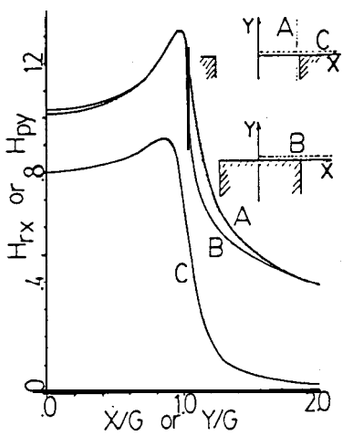

FIG. 7 Comparison of the write field distribution between a ring head and a pole type head. Curve A: H_{Rx} vs y/g, parallel to its symmetric plane; Curve B: H_{py} vs x/p (p=g=1), along the direction of the media motion. Curve C: H_{Rx} vs x/g, along the direction of the media motion. Curves A and B are equivalent but not identical. All the curves are O.lg off the head surfaces.

minor modification to Eqs. (5) and (6). Referring to Fig. 8 we have*

$$H_{Rx} = H_0 + \sum_{n=1}^{\infty} A_n \frac{2n\pi}{G} \cos\frac{2n\pi x}{G} \cosh\frac{2n\pi y}{G} / \cosh\frac{n\pi L}{G} ,$$

in region A, (12a)

$$H_{RX}^{C} = \frac{H_0}{\pi} [\tan^{-1}(\frac{x + G/2}{y - L/2}) - \tan^{-1}(\frac{x - G/2}{y - L/2})] +$$

$$\sum_{n=1}^{\infty} A'_n \frac{4n(-)^n}{G} \int_0^{\infty} \frac{k\sin(kG/2)\cos kx}{k^2 - (2n\pi/G)^2} e^{-k(y-L/2)} \, dk ,$$

in region C. (12b)

We only need to rotate the coordinate system anticlockwise by $\pi/2$, setting $y \to x$, $x \to -y$ and $G/2 \to d$ to obtain the corresponding pole type head write field with ease. Of course, we have the same problem noted above because they refer to different write field spaces.

IV. GENEALIZED POISSION INTEGRAL AND HEAD FIELD CALCULATION

Previously we noted the usefulness of using a rational parametric equation, Eq. (11), incorporated with the Poisson integral to express a ring head field function in the half-space above the head surface. In this section we show that the Poisson integral can be easily extended to express the head field function anywhere in space both within and outside the gap.

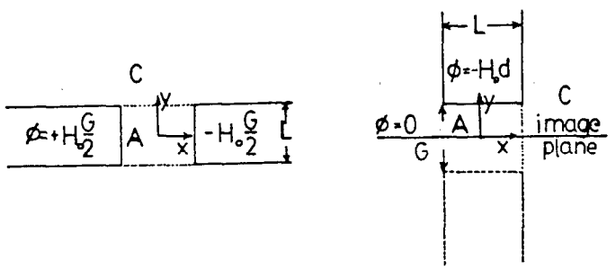

FIG. 8 (a)Configuration of a ring head with a finite pole piece. L: pole thickness; G = gap width. (b)Configuration of a pole type head with spacing d = G/2 and a keeper layer at y = 0.

region. Following Szczech et al[7] and taking a contour integral C along the head pole surfaces as indicated in Fig. 9, we have

$$H_x(x', y') = \frac{1}{2\pi}\int_c [H_y(x,y)K_1 + H_x(x,y)k_2\ 3\ dx + \frac{1}{2\pi}\int_c [H_x(x,y)K_1 - H_y(x,y)K_2\ 1\ dy, \tag{13a}$$

$$H_y(x', y') = \frac{1}{2\pi}\int_c [H_x(x,y)K_1 - H_y(x,y)K_2\ 1\ dx + \frac{1}{2\pi}\int_c [H_y(x,y)K_1 + H_x(x,y)K_2\ 1\ dy \tag{13b}$$

where

$$K_1 = \frac{x - x'}{(x - x')^2 + (y - y')^2}, \quad K_2 = \frac{Y - y'}{(x - x)^2 + (y - y')^2} \tag{13c}$$

and on S_1

$$H_x^{(S_1)} = (t, L/2) = A_1 + B, G^2/[(C_1 G)^2 - t^2], \quad H_Y^{(S_1)}(t, L/2) = D_1 tG/[(E_1 G)^2 - t^2] \tag{14a}$$

and on S_2

$$H_x^{(S_2)}(G/2, t) = A_2 + B_2 L^2/[(C_2 L)^2 - t^2], \quad H_y^{(S_2)} \equiv 0 \tag{14b}$$

and the corresponding efpressions for the field components on S_1' and S_2', respectively. The determination of these 8 parameters A, , B_1, C_1, D_1, E, , A_2, B_2 and C_2 will greatly simplify the calculation of the head field components. Not surprisingly, A, , B_1 and C_1 turn Out to be identical to A, B and C as listed in Table I for pole thickness-to-spacing ratios $\geqslant 4$. Figure 10 shows the distribution of the x-component of the field at several y values below

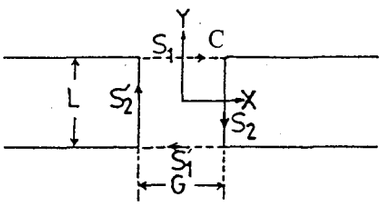

FIG. 9 Contour C for the calculation of the extended poisson integral.

the gap face at G = 1, based on the extended Poisson integral Eq. (13) in comparison with the Fourier series calculations with n = 200. Overall, the extent of agreement between the two sets of curves is reasonably good. The worst relative deviation which shows up in the curves nearest the surface at y ≅ 0.4 at the gap center is 2.9%. Note that the H_x (0, y) value along the symmetric line (the y-axis) is always less than the deep gap field H_0 (H_0 is normalized to unity) while that of the $H_x(\pm G/2, y)$ is greater than it. This statement is valid for any ring heads. Alternatively, by equating the magnetizing field just outside the head

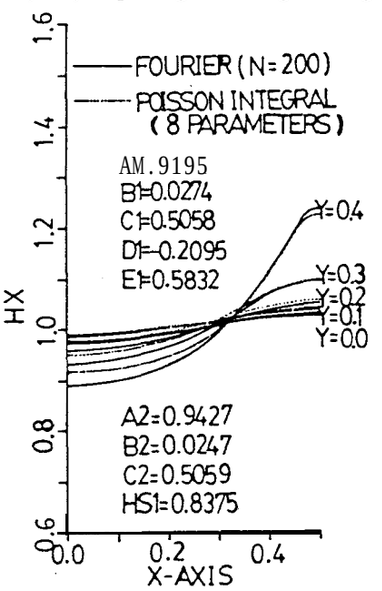

FIG. 10 The distribution of the x-component of field at several y values below the gap face at g = 1 based on the extended poisson integral, in comparison with the Fourier series calculation at n = 200.

pole surface to the magnetization vector

$$H_{(out)}(x, Y) = 4\pi \mathbf{M}_{(in)}(x, Y) \tag{15}$$

eqs. (13a) and (13b) can be reduced to (in cgs)

$$H_x(x', y') = -2 \int_{C'} M \cdot nK_1 \, dx - 2 \int_{C'} \mathbf{M} \cdot nK_2 \, dy \tag{16}$$

with

$$4\pi M_x^{(S_2)} = A_3 + B_3 L^2/[(C_3 L)^2 - y^2\ ],\ M_y^{(S_2)} = 0 \tag{16a}$$

$$4\pi M_y^{(S_1)} = D_3 Gx\ /\ [(E_3 G)^2\ - x^2\ ],\ M_x^{(S_1)} = 0\ , \tag{16b}$$

by taking a proper contour C ' shown in Fig. 11. Thereby the head field distribution can be obtained self-consistently via an iteration scheme[9]. In this calculation only a total of 5 parameters are needed. The values of these parameters vary slightly depending on the range of the integration limits taken for S_1 (measured from the gap center). A typical plot of the x-component of the field distribution above the gap surface corresponding to $S_1 = 4G$ is

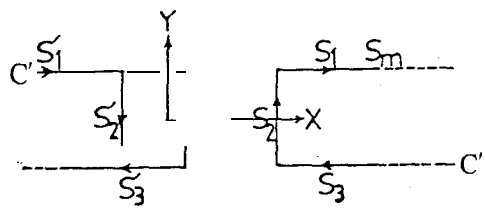

FIG. 1 1 Contour C ' for self-consistent calculation of the extended poisson integral

shown in Fig. 12. The results from FEM calculations which divides the head pole surfaces S, and S_2 into 100 by 100 elements are also shown for comparison. The agreement between the two sets of curves is excellent at low spacings. Thus, with the five parameters evaluated (for a chosen range of the integration limits S_1) the method of the extended Poisson integral is capable of computing the magnetic field distribution with great precision in a simple and easy way.

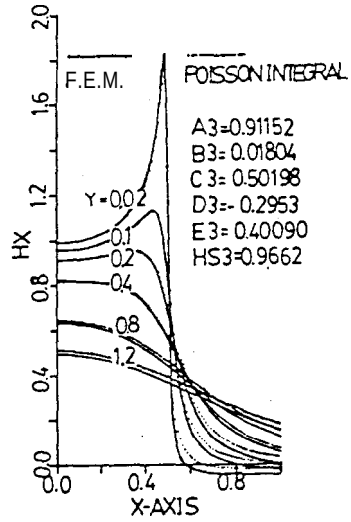

FIG. 12 A typical plot of the ring head write field distribution at several spacings based on the self-consistent calculation of Eq. (16). An FEM calculation result is also shown for comparison. The inset parameters correspond to the optimum choice for self-consistancy.

V. CONFORMAL MAPPING AND THIN FILM HEADS

A ring head with gap length g lying between two poles of potential difference $-H_g g/2$ and $H_g g/2$ along the x-axis in the z-plane may be transformed into a straight line along the U-axis in the W-plane with a line current source of strength $H_g g$ passing through the origin at U = 0 as shown in Fig. 13. The potential, function due to the line current $H_g g$ may be expressed as

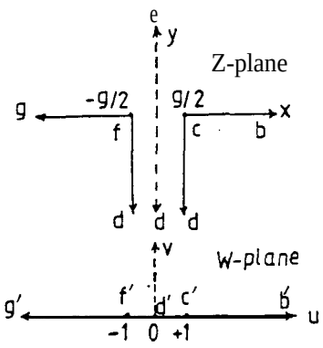

FIG. 13 Transformation of a ring head in the z-plane to a straight line in the W-plane with a line current of strength $H_g g$ passing through the origin at u = 0.

$$\phi = \frac{H_g g}{\pi}(\theta - \pi/2), \quad \text{with } \theta = \tan^{-1}(v/u) \tag{17}$$

Thus, in the W-plane,

$$H_x - j H_y = -\frac{d\phi}{dz} = \frac{d\phi}{dw}\cdot\frac{dw}{dz} \tag{18}$$

with

$$\Phi(w) = -j \frac{H_g g}{\pi}(\ln W - j\frac{\pi}{2}) \tag{19}$$

In the presence of a magnetic charge we resort to the Green function G to obtain the proper potential function Φ. We have

$$\Phi(z) = \int\int \rho(x', y')\, G(W, W')\, dx'\, dy' \tag{20}$$

with

$$G(W, W') = -2 \ln | W - W' | + 2 \ln | W - W'^* | \tag{21}$$

where W' and W'* are the position of the charge and its image respectively, and

$$dZ/dW = (g/n) \cdot \sqrt{W^2 - 1} / W \quad (22)$$

Give a particular geometric configuration one should be able to obtain the corresponding Green function, hence the potential function and the head field distribution through eq. (18). In a problem of practical interest, the inverse mapping function is not frequently easily reducible to an analytic (closed) form. To facilatate calculation, the gapped ring head is then approximated by a simple slot plane of zero depth of the same gap length g[23]. With this approximation we obtain the x-component of field as

$$H_x = H_0 + \mathrm{Re} \iint \rho\,(x', y')\,(K_2 - K_0)\,dx'\,dy' \quad (23)$$

with the Green function $K_2 - K_0$ given by

$$K_2 - K_0 = \frac{2}{\pi g}\left(\frac{W^2}{W^2 - 1}\right)\frac{W' - W'^*}{(WW' - 1)(WW'^* - 1)} \quad (24)$$

Note that the correct factor $(2/\pi g)$ is given here, instead of the factor $(4/\pi g)$ as erroneously given elsewhere[24].

Figure 15 shows the demagnetization field of an arctangent transition in free space (a), in front of an infinitely permeable plane (b), and in the presence of a gapped infinite ring head (c). By comparing (a) and (b) we notice that the presence of an image charge has the net effect of cutting down the demagnetization field. For a gapped head the demagnetization field becomes more negative or less positive at the position where the charge sits while at the same time a shoulder is introduced into the field distribution on the far side of the gap edge. The latter effect is much less pronounced than reported elsewhere[24], perhaps due to the presence of the different prefactor, $2/\pi g$, instead of $4/\pi g$, in eq. (24) as mentioned earlier.

In the case of a thin film head with gap length g and of pole tip p, one can proceed as follows[25] (Fig. 14).

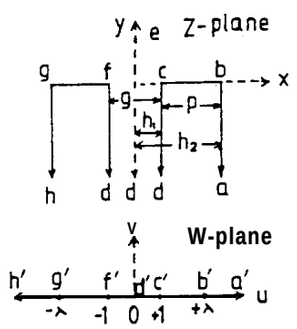

FIG. 14 Transformation of a thin film head system in the z plane to a straight line in the w plane'.

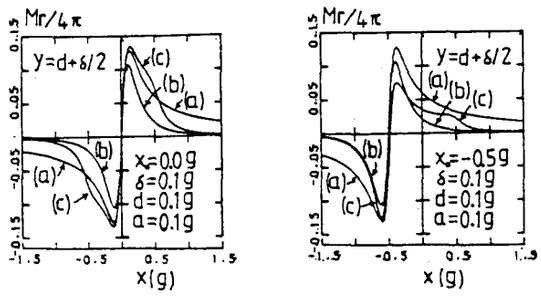

FIG. 15 Demagnetization field of an arctangent transition: a) in free space b) in the presence of an infinitely permeable plane, c) in the presence of a gapped head of infinite permeability.

Letting $h_1 = g/2$, $h_2 = p + g/2$, the positions on the x-axis in the z-plane $(h, 0)$, $(h_1, 0)$, $(0, 0)$, $(-h_1, 0)$ and $(-h_2, 0)$ may be transformed to the u-axis on the w-plane as $(h, 0)$, $(1, 0)$, $(0, 0)$, $(-1, 0)$, $(-\lambda, 0)$. We then have

$$Z = Z_0 + A\left\{(W^2-1)^{1/2} - \left(\frac{1+\lambda^2}{2}\right) \times \ln[(W^2-1)^{1/2}(W^2-\lambda^2)^{1/2} + W^2\frac{1+\lambda^2}{2}] + \lambda \ln\left[\frac{(W^2-1)^{1/2}(W^2-\lambda^2)^{1/2} + \lambda\frac{1+\lambda^2}{2}}{W^2}\right]\right\} \tag{25}$$

where the real part and the imaginary part of z_0 are, respectively,

$$Z_{or} = h_1(1+c), Z_{oi} = -\frac{h_1}{\pi}[\ln(c^2-1+c(c^2-1)^{1/2}) + \ln(c^2-1)^{1/2}],$$

and

$$A = -\frac{i}{\pi}\frac{h_1}{c+(c^2-1)^{1/2}}, \quad h_1 = g/2,\ c = 1 + 2p/g,\ \lambda = c + (c^2-1)^{1/2} \tag{26}$$

In Fig. 16 we show in solid lines the plot of the x-component of the thin film head field at various flying heights for $p = g$. The field distribution in a region between the gaps above the head is practically similar to the Fan field, while outside the gap and beyond the pole tip, it turns quite dissimilar and becomes negative.

To carry out the actual calculation for, the thin film head field via the Christoffel-Schwarz transformation method is, however, not always an easy matter, because there is no easy way to find the inverse mapping function W(z). To simplify the procedure, an ingenious parametric field equation, similar to that given for the ring head, was recently proposed[26], giving

$$H_x(t, 0) = \begin{cases} [A + \dfrac{Bg^2}{(cg)^2 - t^2}]\ Hs, & -g/2 \leqslant t \leqslant g/2; \\ 0 & g/2 < t < g/2+p; \end{cases} \tag{27}$$

$$\left\{ \left[\frac{gD}{(\frac{g}{2} + p)E - t} \right] Hs \,, \qquad t \geqslant g/2 + p \right. \quad .$$

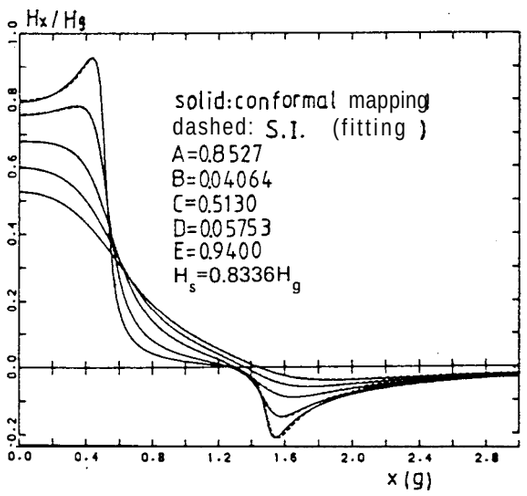

FIG. 16 The x-component thin film head field at several spacings for p = g. Solid lines: conformal mapping, dashed lines: parametric field equation using eq. (27).

The dashed lines in Fig. 16 show the results of the calculation from substituting eq. (27) for eq. (9) by least square fitting the parameters for A, B, C, D and E as listed below:

P = (g)	D	D
1.0	0.05753	0.9400
1.5	0.05640	0.9415
2.0	0.05530	0.9430

Approximately, the parameters D and E can be expressed as

$$D = -0.00223\ (p/g) + 0.05976$$
$$E = 0.0030\ (p/g) + 0.9370$$

while the parameters A, B and C are unchanged from those given previously. Figure 17 shows, comparison of the result of similar calculations for p = g, 1.5g and 2.0g. Clearly, the calculation using the parametric equation is as good as can be expected.

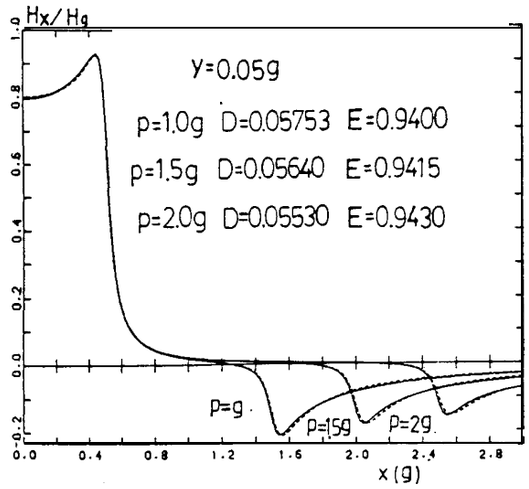

FIG. 17 The x-component thin film head field at p = g, 1 .5g and 2.0g. Solid lines: conformal mapping, dashed lines: parametric field equation.

VI. MAGNETORESISTIVE HEADS

The operational principle of a magnetoresistive (MR) head can be stated as follows: The effective magnetoresistance change in the MR element and the demagnetization field H_y produced by magnetic reversals in the storage medium are related by

$$\Delta \rho/\rho = (\Delta\rho/\rho)_{max} \sin^2 \theta \tag{17}$$

$$H_y = H_0 \sin 0 \tag{18}$$

where $H_0 = N_y M_0 + H_k$, N_y being the demagnetization factor of the MR element, M_0 is the saturation magnetization, H_k is the anisotropic field, and θ is the angle between M and the current density vector J in the MR element (see Fig. 18). Upon application of an appropriate bias field to maintain optimum sensitivity at $\theta \sim \pi/4$, a linearized readout variable voltage AV can be expressed as[13]

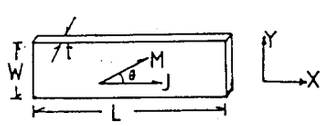

FIG. 18 Configuration of an MR element.

$$AV \cong -(\sqrt{2}\, JL\Delta\rho/H_0)\, H_y \tag{19}$$

Much of the work on MR heads is related to the evaluation of H_y, enhancement of the signal-to-noise (SN) ratio and increasing the signal resolution. The latter is usually effectively accomplished by providing magnetic shields to the MR element[14], known as the shielded MR heads (see Fig. 19). Alternatively, it maybe approached from either the time domain[15] or the frequency domain[16] compensation scheme, by the delay-line approach[17] or by the so-called cosine equalizer[18]. In order to increase the SN ratio shielded dual-element MR heads with different circuital arrangement and sensing schemes[19] have been devised to cut down thermal noise with considerable success. Presently we will discuss mainly the shielded MR head, while the yoke MR head[20] and the barber pole head[21] will not be touched.

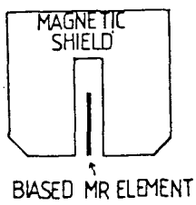

FIG. 19 Configuration of a shielded MR transducer.

VII. UNSHIELDED MR HEADS

The average readout signal field maybe approximated as

$$H_y(\bar{x}) = \frac{1}{w\,t} \int_{x-t/2}^{\bar{x}+t/2} dx \int_{d+\delta/2}^{d+\delta/2+w} H_y(x, y)\, dy \tag{20}$$

where $H_y(x, y)$ given by Eq. (18), is the demagnetization field due to magnetization reversal in the storage medium. For an isolated arctangent transition,

$$M = -\frac{2M_r}{\pi} \tan^{-1}\frac{x}{a}$$

$$H_y(x, y) = \frac{Mr}{2\pi} \mathrm{Ln}\, \frac{x^2 + (y + \delta/2 + a)'}{x^2 + (|y - S/2\ I + a)^2} \tag{21}$$

VIII. SHIELDED MR HEADS

A typical MR head configuration and its corresponding magnetic potential is shown in

Fig. 20. Since the hed gap length is relatively narrow, the magnetic scalar potential f(x) versus g is approximately linear, the head system maybe looked upon as two ring heads in

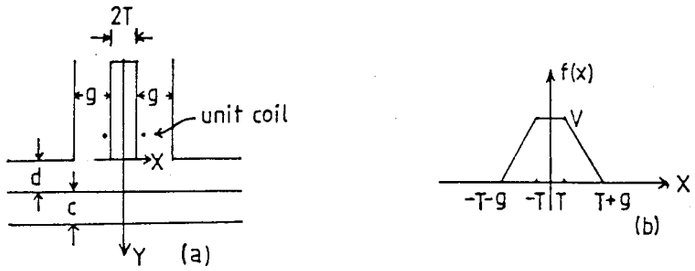

FIG. 20 Coordinate system and magnetic potential of a shielded MR head.

series. We have[14]

$$f(x) = f_0(x+\frac{g}{2}+T) - f_0(x-\frac{g}{2}-T) \tag{22}$$

The corresponding head gap field $\mathbf{H}_h(x, y)$ may be written as

$$\mathbf{H}_h(x, y) = \mathbf{H}_{h0}(x+\frac{g}{2}+T, y) - \mathbf{H}_{h0}(x-\frac{g}{2}-T, y) \tag{23}$$

where $\mathbf{H}_{h0}$ is the head gap field due to a conventional ring head. The average induced flux as sensed by the MR element is

$$\phi(x) = \int_d^{d+\delta} dy \int_{-\infty}^{\infty} \mu_0 LM(x-\bar{x}, y) H_x(x, y)\, dx$$

$$= \phi_{h0}(\bar{x}+\frac{g}{2}+T) - \phi_{h0}(\bar{x}-\frac{g}{2}-T)$$

$$= \frac{1}{v}\int_{-\infty}^{\bar{x}} [e(x+\frac{g}{2}+T) - e(x-\frac{g}{2}-T)]\, dx \tag{24}$$

in which e(x) is the readout signal from a ' conventional ring head at the position x, and v is the relative volocity of the head-media system. Alternatively, by expressing the magnetic scalar potential $\phi(x, y)$ in terms of a 2-dim Green function and the surface scalar potential f(x) by

$$\phi(x, y) = \frac{y}{\pi}\int_{-\infty}^{\infty} f(t)\frac{1}{y^2+(t-x)^2}\, dt \tag{25}$$

the induced voltage can be written as[22]

$$E(\bar{x}) = \frac{K}{\pi}\int_d^{d+\delta} dy \int_{-\infty}^{\infty} dx \int_{-\infty}^{\infty} dt \frac{yf(t)}{y^2+(t-x)^2}\frac{\partial M}{a_x} \tag{26}$$

where K is an appropriate constant and the magnetic surface scalar potential f(x) is

$$f(t) = \begin{cases} V + \dfrac{VT}{g} - \dfrac{V}{g}\,t\,, & T \leqslant t \leqslant T+g \\ V\,, & -T \leqslant t \leqslant T \\ V + \dfrac{VT}{g} + \dfrac{V}{g}\,t\,, & -T-g \leqslant t \leqslant -T \\ 0 & \text{otherwise} \end{cases} \tag{27}$$

The equivalent head field function can be easily obtained via

$$\mathbf{H}(x, y) = -\Delta\phi(x, y) \tag{28}$$

For a thin film disk at low spacings (or in contact reading) the head field function may be reasonably approximated as

$$H_y(x, y) = \frac{M_r}{2\pi^2} \int_{x-g-T}^{x+g+T} \frac{a}{x'^2 + a^2}\, \mathrm{Ln}\, \frac{(y + \delta/2)^2 + (x - x')^2}{(y - \delta/2)^2 + (x - x')^2}\, dx' \tag{29}$$

Figure 21 shows the half-width distribution of the head field function versus gap width g corresponding to Eqs. (23), (28) and (29), denoted respectively as methods 1, 2, and 3, at the prescribed input data. For narrow gap widths curves from the three methods agree

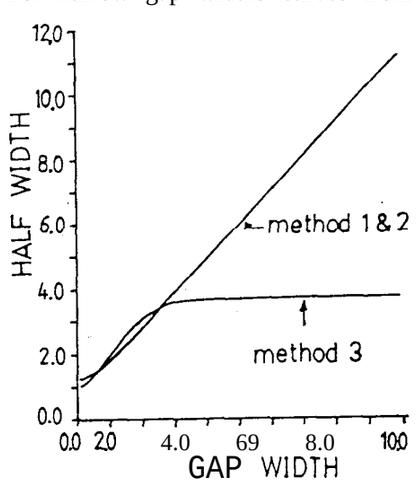

FIG. 21 Comparison of the half width distribution versus gap width variation corresponding to Eq. (23), (method 1), Eq. (28) (method 2) and Eq. (29) (method 3) for a shielded MR head.

reasonably well, with the first two methods virtually yielding identical set of curves. As the gap-width broadens the curves start to part company with only method 3 showing signs of a saturation effect. Figure 22 shows comparison between the two sets of curves. If both

the coating thickness and spacing are small the two curves show reasonable agreement, as show in Fig(a). Otherwise the relative deviation becomes substantial as reflected in Fig. (b).

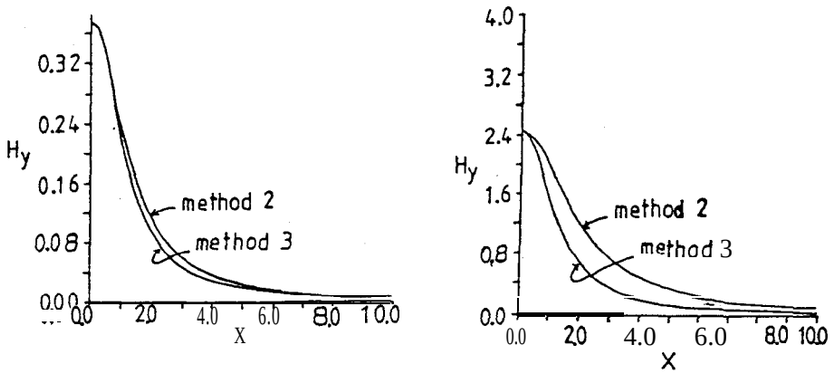

FIG. 22 Comparison of the y-component of the head field between methods 1 and 3. (a) Both the coating thickness and spacing are small. (b) Either coating thickness and/or spacing are not small.

In summary, the methods described above all yield reasonably good results at high density readouts whenever the gap-width is narrow. However, when it becomes width the methods (1) and (2) fail badly because the linearity assumption between the magnetic surface scalar potential versus the gap-width is no longer valid. By comparison, Eq. (29) yields correct results at any gap-width values as long as the effective spacing, i.e., spacing plus media thickness, is small.

REFERENCES

1. I. A. Beardsley, "Modeling the record process", IEEE Trans Magn Vol. Mag-22, 454, 1986.
1a. A. S. Hoagland "Digital Magnetic Recording", Wiley, 1963, New York, page 62; See also H. N. Bertram, proceedings of IEEE Vol. 74, No. 11, 1494, Nov. 1986.
2. 0. Karlquist, "Calculation of the magnetic field in the ferromagnetic layer of a magtic drum " Trans. Roy. Inst. Tech. Stockhdm 86, 3, 1954.
3. H. L. Huang. "Two dimensional Green's function and Karlquist's equation" Chin. J. Phys. 20,106, 1982.
4. G. J. Fan, "A study of the playback process of a magnetic ring head" IBM J. Res. Devel, Oct. 32 1, 196 1.
5. H. L. Huang and H. Y. Deng "Magnetic fields of ring head and pole type head." J. Magn Magn Mats. 54-57, 1661, 1986.
6. H. L. Huang and H. Y. Deng, "Comparison of ring head and SPT head write fields", IEEE Trnas. Magn. Vol. MAG22, 1305, 1986.
7. T. Szczech, D. Perry and K. Polmquist, "Improved field equations for ring heads",

IEEE Trans. Mag. Vol. Mag-19, 1740, 1983.
8. H. L. Huang and S. C. Yen, "On the equivalence of ring and pole-keeper heads", Jpn J. Appl. Phys., 25, 1552, 1986.
9. H. L. Huang and S. C. Yen, "Generalized Poisson Integrals and parametric head field equation", J. Appl. Phys., 60, 4015, 1986.
10. G. J. Fan, "Analysis of a practical perpendicular head for digital purposes", J. Appl. Phys., Suppliment 31, 402s, 1960.
11. J. C. Mallinson and H. N. Bertram, "On the choracteristics of pole-keeper head fields", IEEE Trans, Magn. Vol. Mag-20, 721, 1984.
12. J. A. Sievers, "Field symmetries and equivalences in longitudinal and perpendicular recording", IEEE Trans. Magn Vol. MAG-19, 1745, 1983.
13. R. P. Hunt "A magnetoresistive readout transducer", IEEE Trans. Mag. Vol. Mag-7, 150, 1971.
14. F, I. Potter, "Digital magnetic recording theory", IEEE Trans Magn, Vol. Mag-10, 502, 1974.
15. "Increased mangetic recording readback resolution by means of a linear possive network".
16. G. J. Jacoby, "Signal equalization in digital magnetic recording", IEEE Trans. Magn Vol. Mag-4, 1986.
17. R. C. Schneider, "An improved pulse-slimming method for magnetic recording", IEEE Trans. Magn Vol. Mag-11, 1240, 1975.
18. T. Tameyama, S. Taka nani, R. Arai, "Improvement of recording density by means of cosine equalizer", IEEE Trans Magn Vol. Mag-I 2, 746, 1976.
19. See for examples F. J. Jeffers, "Magnetoresistive Transducer with canted easy axis", IEEE, Trans Magn Vol. Mag-15, 1628, 1979.;
F. B. Shelledy, G. W. Brock, A linear self-biased magnetorsistive head, IEEE. Trans. Magn. Vol. Mag-11, 1296, 1976.;
F. B. Shelledy and S. D. Chestham, "Suppresion of thermally induced pulses in magnetoresistive heads", IERE Conf. proceeding, No. 15, 251, 1976.
20. W. F. Druyvesteyn; J. A. C. Van Ooyen, L. Postma; E. L. M. Raemaekers, J. J. M. Ruigrok; J. de Wilde, "Magnetoresistive Heads", IEEE Trans Magn, Vol. Mag-17, 2884, 1981.
21. K. E. Kuijk, W. J. Van Gestel, F. W. Gorter, "The barber pole, A linear magnetoresistive head", IEEE Trans Magn Vol. Mag-11, 12 15, 1975.
22. A. V. Davies and B. K. Middleton, "The resolution of vertical magneto-resistive readout heads", IEEE Trans. Magn Vol. Mag-11, 1689, 1975.
23. D. A. Lindholm,. "Image fields for two-dimensional recording heads", IEEE Trans. Magn. Vol. MAG-13(5), 1463, 1977.
24. ibid, equation (5).
25. J. S. Yang and H. L. Huang, to be published.
26. T. J. Szczech and P. R. Iverson, "An approach for deriving field equations for magnetic heads of different geometrical configurations", IEEE Trans. Vol. Mag-22, 355, 1986.